

# Sonication-Triggered Rolling of Janus Porous Nanomembranes for Electrochemical Sensing of Dopamine and Ascorbic Acid

Fei Ma, Bin Yang, Zhe Zhao, Yuting Zhao, Ruobing Pan, Dingrun Wang, Ye Kong, Yimeng Chen, Gaoshan Huang,\* Jilie Kong, and Yongfeng Mei\*



Cite This: <https://dx.doi.org/10.1021/acsnm.0c02019>



Read Online

ACCESS |



Metrics & More

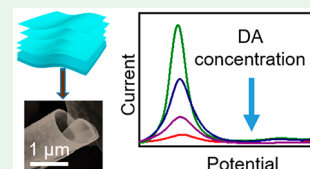


Article Recommendations



Supporting Information

**ABSTRACT:** Selective electrochemical sensing of dopamine and ascorbic acid has great importance to address the issue associated with neurological disorders including Parkinson's and Alzheimer's diseases. In this work, we combine atomic layer deposition with sonication technique to produce metal oxide microtubes. The Janus nanomembranes deposited on a sponge template with single-side porous structure are triggered to roll under the sonication. The influence of the nanomembrane thickness, the post-treatments, and the solvent polarity have been investigated, and the results demonstrate the universality of the current approach in fabricating microtubes from different oxides Janus nanomembranes. In addition, microtubes after functionalization are used for electrochemical sensing of dopamine and ascorbic acid. The fabricated DA sensors exhibit great selectivity and sensitivity with an ultralow limit of detection ( $0.025 \mu\text{M}$ ) and a wide detection range ( $0.4\text{--}80 \text{ mM}$ ) due to their tubular structures, the porous inner surfaces, and the exposure of active sites. The microtubular sensor maintains a stable sensing performance after 12 days. This sonication-triggered rolling process has potential in producing various 3D microstructure and therefore may have important applications in future micro-/nanodevices.



**KEYWORDS:** atomic layer deposition, Janus, porous, nanomembrane, rolling, biosensor, dopamine, ascorbic acid

## INTRODUCTION

Morphology plays a major role in programming the function of materials.<sup>1–3</sup> For instance, owing to the difference in shape and dimension, the properties of fullerenes, graphene, and carbon nanotubes are quite different from each other.<sup>4,5</sup> Consequently, their potential applications are quite different.<sup>6</sup> Specifically, dimension conversion of nanosheets often results in some unexpected properties, such as optical properties,<sup>7,8</sup> mechanics characters,<sup>9</sup> and electrical behaviors.<sup>10–13</sup> Tubular structures made from oxides, such as  $\text{TiO}_2$ ,  $\text{Al}_2\text{O}_3$ , and  $\text{ZnO}$ ,<sup>14</sup> demonstrate more active sites in comparison with their nanowire/rod counterparts and have recently been widely used in energy applications and sensors.<sup>15–19</sup> For example, hollow microtubes were prepared with large specific surface and the novel surface morphology, which have potential applications in the fields of catalysis, sensors, and drug delivery.<sup>18</sup> In the field of electrochemical sensing, many previous reports have demonstrated that the morphology also plays a crucial role in sensing performance,<sup>20–22</sup> and the enhanced electrochemical properties depend on not only the material intrinsic characteristics but also the morphology and geometry.<sup>23</sup>

It is worth noting that some biomolecules with important physiological function of human body (e.g., dopamine (DA) and ascorbic acid (AA)) exist in the body with very low concentrations. Hence, highly sensitive detection is of importance for medical treatment. Previously, researchers have been devoted to fabricating high performance biosensors by using different active materials and composites.<sup>24,25</sup> For

instance, Qing et al.<sup>24</sup> fabricated polypyrrole-loaded PVA-co-PE nanofibers for dopamine monitoring. Reddy et al.<sup>21</sup> used dopamine modified carbon nanotubes as dopants of poly(3,4-ethylene dioxathiophene) to prepare hybrid films for biosensing. These researchers, however, generally prepared flat electrochemical sensors with active materials on the outer surface. We consider that the biosensors with active material in microtubular geometry which can confine target biomolecules should possess enhanced device performance and thus may have great potential.

So far, a considerable number of different strategies have been developed to prepare tubular structures.<sup>5,26–30</sup> The main routes can be roughly divided into intercalation/exfoliation procedure,<sup>31</sup> self-rolling method,<sup>32,33</sup> and template-growth technique.<sup>34</sup> Such methods can produce tubular structures commonly under rigorous conditions like liquid nitrogen or strong chemical solvents, and few can transform the shape under the mild water condition. Herein, we report a facile protocol to roll Janus porous nanomembranes fabricated by atomic layer deposition (ALD). In this approach,  $\text{TiO}_2$ ,  $\text{ZnO}$ , and  $\text{Al}_2\text{O}_3$  nanomembranes were deposited by ALD on polyurethane sacrificial template. After heat treatment and

**Received:** July 24, 2020

**Accepted:** September 22, 2020

**Published:** September 22, 2020

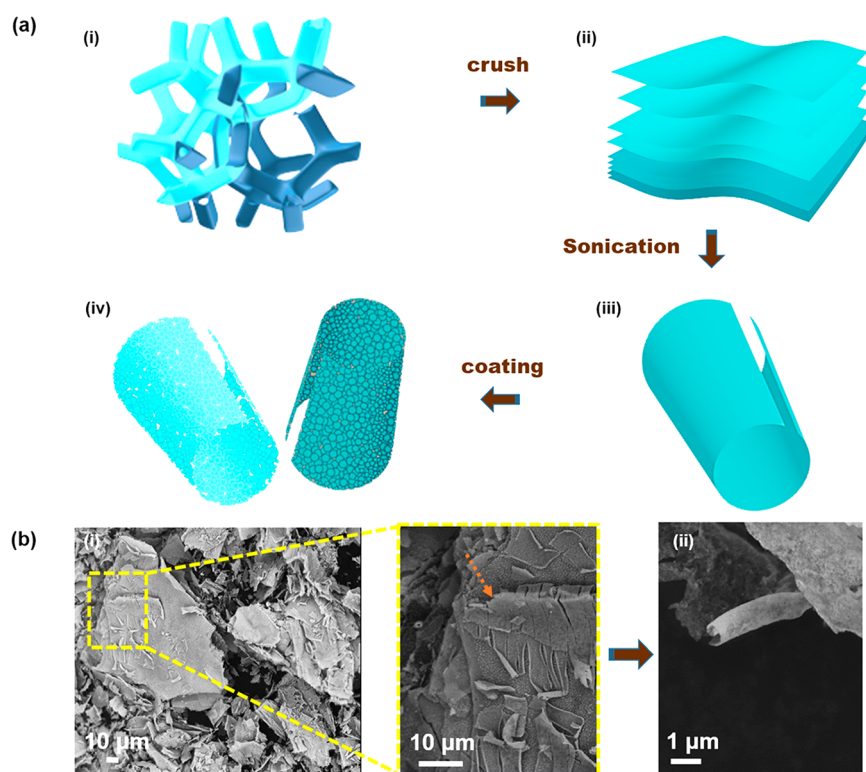


**Figure 1.** (a) Schematic of the fabrication process of metal oxide microtube. (b) SEM image in (i) shows stacked TiO<sub>2</sub> nanomembranes. The yellow rectangle highlights a nanomembrane that starts to roll under ultrasonication treatment. SEM image in (ii) demonstrates a typical TiO<sub>2</sub> microtube.

the removal of the polyurethane template, a large number of nanomembranes were obtained. Self-rolled microtubes were then obtained under the sonication post-treatment. We present a systematic study of the influence of environmental conditions (e.g., temperature of solvent, effects of nanosheets thickness, and polarity of solvent) on the rolling process. The electrochemical properties of the microtube and corresponding sensing applications were investigated, and excellent sensing selectivity and sensing linearity were observed in our experiment. We consider that the unique tubular structures with a hollow feature and corresponding effective electrolyte diffusion therein lead to the enhanced sensing performance. Such an approach of rolling Janus porous nanomembranes holds considerable promise for electrochemical detection and sustainable environmental applications.

## RESULTS AND DISCUSSION

Figure 1 illustrates the fabrication route of functional microtubes. First, oxide nanomembrane is obtained by ALD process.<sup>35</sup> In this process, oxide nanomembranes with different thicknesses are deposited on the sponge (porous polyurethane) skeleton (Figure S1). The sponge template has porous structure, and the surface of polyurethane contains C=O groups which are beneficial to the growth of oxide during initial ALD.<sup>36,37</sup> Then, the sponge template is removed by a high temperature annealing process in O<sub>2</sub>. Only the oxide skeleton that duplicates the structure of the template is left, and the complex 3D network-like structure is retained (Figure 1ai). The metal oxide skeleton is then crushed to produce a large amount of metal oxide porous nanomembranes (Figure 1a ii). Subsequently, metal oxide nanomembranes are subjected to an ultrasonication process. The synergy effect from surface

tension of water and ultrasonication leads to rolling of the nanomembranes into hollow microtubular structures (Figure 1a iii and Figure S1). Different sensing microtubes were then prepared by coating active materials onto the wall of microtubes (Figure 1a iv). More scanning electron microscopy (SEM) images of TiO<sub>2</sub> nanomembranes on sponge, free-standing TiO<sub>2</sub> nanomembranes, and TiO<sub>2</sub> microtubes fabricated with different ALD cycles can be found in Figure S1. In order to prove the versatility of the current approach, various oxide nanomembranes were subjected to ultrasonication treatment. Figure 2 shows SEM images of ZnO (200 ALD cycles), TiO<sub>2</sub> (400 ALD cycles), and Al<sub>2</sub>O<sub>3</sub> (600 ALD cycles) nanomembranes and corresponding microtubes formed. It is evident that all these metal oxide nanomembranes can grow uniformly on the surface of sponge (panels designated as (i) in Figure 2a–c) to produce uniform oxide nanomembranes (panels designated as (ii) in Figure 2a–c), and after sonication, all three kinds of nanomembranes roll into microtubular structures (panels designated as (iii) in Figure 2a–c). The results here indicate that this approach is universal and is capable of fabricating microtubes made from various materials.

The self-rolling process was specifically investigated. As shown in Figure 1bi, before ultrasonication, the TiO<sub>2</sub> nanomembranes stack together due to van der Waals effect. During the ultrasonication process, the stack of nanomembranes are intercalated with water molecular and the force from ultrasonication further leads to the separation and rolling of the nanomembranes (see the arrow in Figure 1bi). With prolonged ultrasonication process, the self-rolling process continues to form a microtubular structure (Figure 1bii). We also carried out TEM characterization of the TiO<sub>2</sub> microtube,

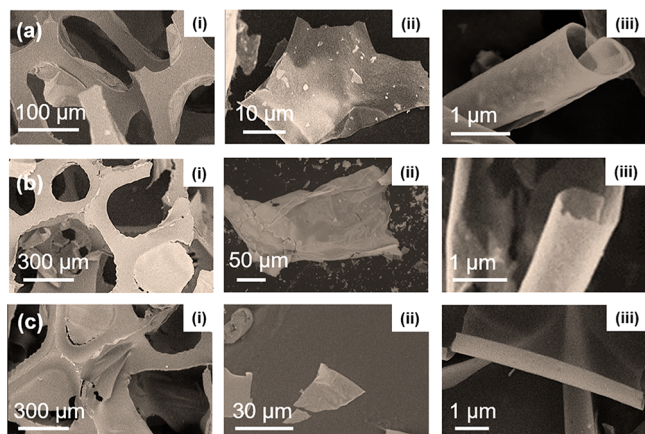


**Figure 2.** SEM images of nanomembranes and corresponding microtubes: (a) 400 ALD cycles  $\text{TiO}_2$  nanomembranes, (b) 200 ALD cycles  $\text{ZnO}$  nanomembranes, and (c) 600 ALD  $\text{Al}_2\text{O}_3$  nanomembranes. Panels designated as (i) are nanomembranes on sponge templates. Panels designated as (ii) are free-standing nanomembranes. Panels designated as (iii) are corresponding microtubes.

and the obtained image is demonstrated in Figure S2. It can be clearly seen that the  $\text{TiO}_2$  nanomembrane with good homogeneity rolled into microtubular structure and the stack of the rolled nanomembrane may remarkably improve the structural stability. We also carried out control experiments to determine whether the sonication step is critical for microtube fabrication. For  $\text{TiO}_2$  and  $\text{ZnO}$  nanomembranes with only soaking or heating treatment, microtubes can hardly be observed (Figures S3 and S4). This indicates that the driving force for the rolling process is mainly from ultrasonication treatment. The influence of solvent polarity on rolling process is also studied in detail. We sonicated nanomembranes in various solvents with different polarities. It was found that 80% of the nanomembrane can roll after sonication (2 h, 100 kHz) in solvent with large polarity (i.e., water), while in solvent with small polarity (i.e., hexane), the possibility of microtube formation is significantly low (Figure S5). We also notice that the thickness of the nanomembrane has an obvious influence on the microtube formation. Figure S1 shows the microtubes fabricated by sonicating  $\text{TiO}_2$  nanomembranes of 100, 200, and 300 ALD cycles. The nanomembranes with 100 and 200 ALD cycles are fragile because the nanomembranes are too thin, and the possibility of microtube formation is relatively low. The nanomembranes with 400 ALD cycles lead to the formation of perfect microtube and therefore will be used for sensing applications in the following part. In order to further investigate the crystal structure and purity of the sample, XRD has been tested, and the obtained pattern is shown in the Figure S6. One can see that all the diffraction peaks are associated with anatase  $\text{TiO}_2$ , demonstrating the good purity of the sample. The elemental composition and chemical states of  $\text{TiO}_2$  microtubes were further investigated by XPS (Figure S7). The high-resolution Ti 2p spectrum located at 458.8 eV and O 1s located at 530.0 eV, proving the presence of Ti and O in the sample.

When a large amount of  $\text{TiO}_2$  microtubes were formed, the microtubes are irregularly dispersed and interlaced with each other to form framework (Figure 3a). Figure 3b shows an enlarged SEM image of the opening of a microtube. It is obvious that the inner wall of the microtube is porous with

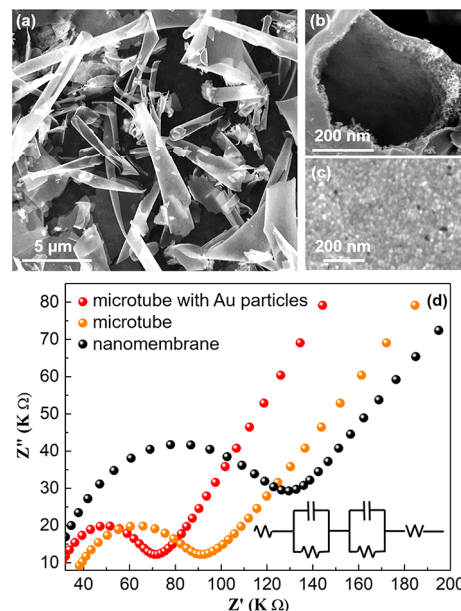


**Figure 3.** (a) SEM image of dispersed microtubes network. (b) Enlarged SEM image of the opening of a microtube where the inner surface can be observed. (c) SEM image of the outer surface of a microtube after the decoration of Au nanoparticles. (d) EIS of electrode made from nanomembranes, microtubes, and microtubes decorated with Au nanoparticles. The inset is the equivalent circuit.

very rough surface. This kind of microtube with single-side porous structure is therefore called a Janus nanomembrane microtube which is due to the aforementioned fabrication process. The sponge template is with the rough surface and the side of the nanomembrane in contact with the sponge template duplicates the surface structure of the sponge, leading to the formation of the unique single-side porous structure. Such a porous structure may have important applications in electrochemistry as the porous structure is beneficial to the penetration and diffusion of the electrolyte while the smooth surface helps to maintain the structural integrity. Figure 3c shows the surface morphology of the outer surface of the microtube after Au nanoparticle deposition. We experimentally proved that the Au particle size can be conveniently tuned by changing the thickness (Figures S8 and S9), demonstrating the controllability of current approach in surface decoration. In the present work, optimized thickness of 4 nm Au was adopted due to the best electrochemical properties.

In our work, electrochemical impedance spectroscopy (EIS) was used to identify the changes of the material's property before and after surface treatment, and the results are shown in Figure 3d. The inset exhibits the corresponding equivalent circuit, and the fitting parameters are displayed in Table S1. Generally, the semicircle in the high-middle frequency corresponds to the charge transfer resistance ( $R$ ). The inclined line in the low frequency represents the Warburg impedance ( $W$ ), which is attributed to the diffusion of ion on the surface of electrode. The electrode current could be divided into two parts in parallel: faradaic current, which is controlled by the charge transfer resistance ( $R$ ) of electrochemical reaction; nonfaradaic current, which is elicited by the charge–discharge of the electrical double layer ( $C$ ).<sup>38</sup> The EIS results indicate that the resistances of the nanomembranes and the microtubes are maintained at a high value. After the Au nanoparticles were deposited, the resistance decreased dramatically (see also

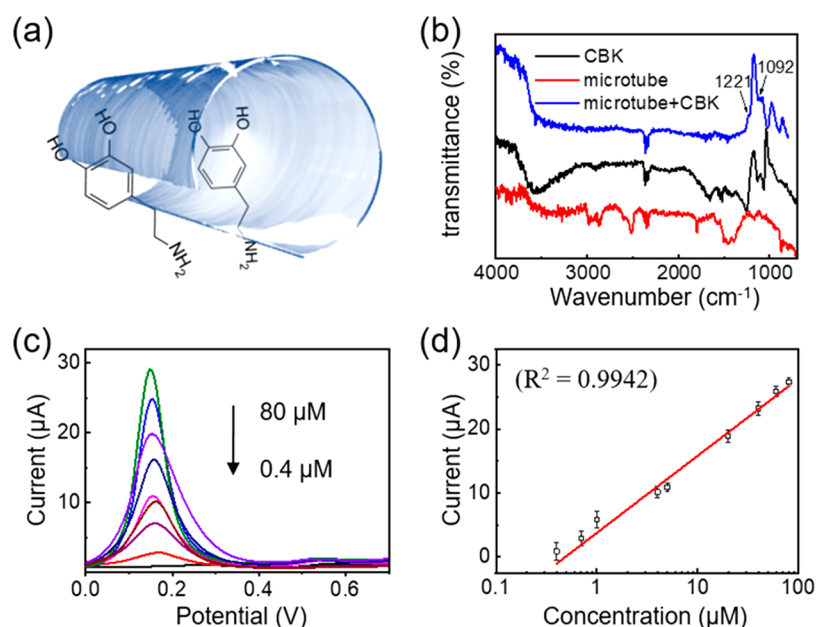


**Figure 4.** Dopamine sensing tests. (a) Schematic of a functional microtube for dopamine sensing. (b) FTIR characteristics of CBK, microtube, and microtube decorated with CBK. (c)  $I$ - $V$  curves of microtube-based sensor to dopamine solutions with different concentrations ranging from 0.4 to 80  $\mu\text{M}$ . (d) Linear fit of the response as a function of dopamine concentration.

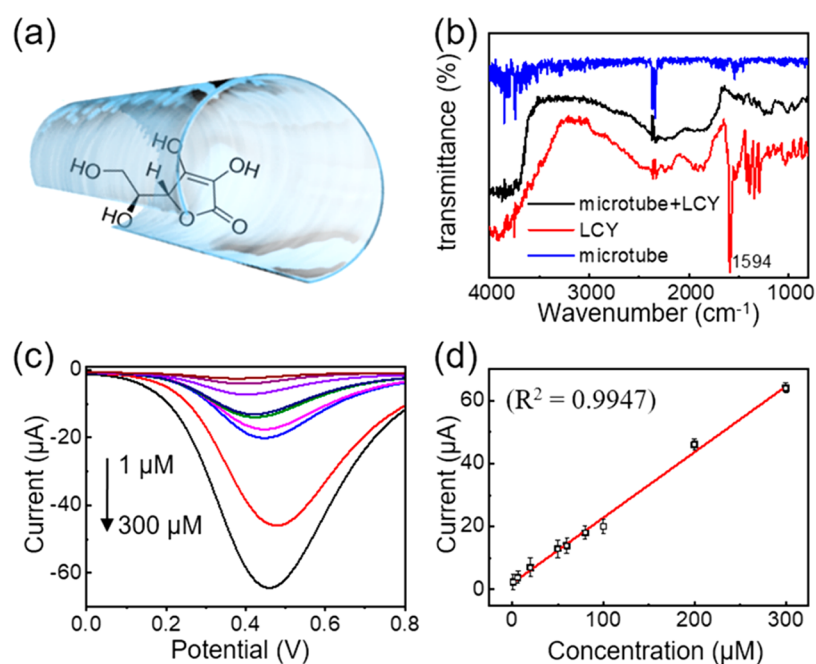


**Figure 5.** Ascorbic acid sensing tests. (a) Schematic of a functional microtube for ascorbic acid sensing. (b) FTIR characteristics of LCY, microtube, and microtube decorated with LCY. (c)  $I$ - $V$  curves of microtube-based sensors to ascorbic acid solutions with different concentrations ranging from 1 to 300  $\mu\text{M}$ . (d) Linear fit of the response as a function of ascorbic acid concentration.

Table S1). This result verifies that the formed Au nanoparticles had high conductivity, which will be helpful in enhanced electrochemical properties. In addition, at the low frequency region, the microtubes with Au particles exhibit the largest slope, indicating the best electrolyte penetration.<sup>2</sup>

The sensor device was assembled by the conjugation of microtube structure and CBK as well as LCY through Au nanoparticles (Figures 4a and 5a). CBK and LCY can specifically bind with DA and AA, respectively, and therefore, the microtube-based sensor can capture the target analytes

selectively. The sensing function can then be realized because the redox reaction should take place after the analytes are attached. In Figure 4b, the Fourier transform infrared (FTIR) spectrum of microtube after surface decoration exhibits absorption peaks at 1221 and 1090  $\text{cm}^{-1}$ , which can be assigned to the stretching vibration of C-O-C in chrome blue K (CBK).<sup>39</sup> This confirms the presence of CBK on the surface of the microtube after surface decoration. The sensor devices were immersed in solution containing dopamine for further electrochemical tests. The response of the sensor was studied

Table 1. Comparison of Biosensing Performance of DA Sensors

sample	LDR ( $\mu\text{M}$ )	DL ( $\mu\text{M}$ )	ref
rGO/TiO <sub>2</sub>	35–100	1.5	41
flake shaped CuO nanoparticles/MCPE Ni(OH) <sub>2</sub> /NiCo-LDHs	0.1–0.01, 0.05–1080	0.055	42
		0.017	43
polychromotrope 2B/GCE	2–80	0.3	44
MWCNT/ $\beta$ -CD/GCE	0–80	6.7	45
TC8A/Au	1–1000	0.5	46
carbon dot	33–1025	500	47
monodispersed Mn <sub>3</sub> O <sub>4</sub> nanoparticles/GCE	1–7	0.1	48
Ag <sub>2</sub> Se quantum dots/GCE	0.5–19	0.1	49
AuNPs@SiO <sub>2</sub> –MIP sensor	0.048–50	0.02	50
TiO <sub>2</sub> microtube	0.4–80	0.025	this work

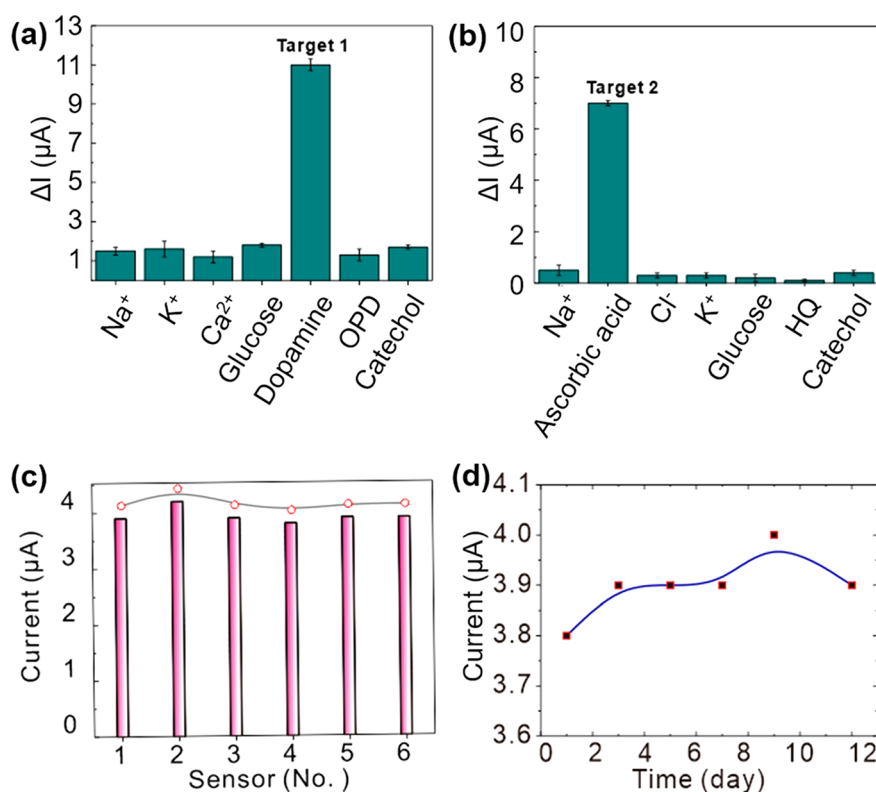


**Figure 6.** (a) Selective response of the microtube-based sensor toward 5  $\mu\text{M}$  dopamine. (b) Selective response of the microtube-based sensor toward 20  $\mu\text{M}$  ascorbic acid. (c) Reproducibility of the sensors. (d) Aging test of the sensor toward 5  $\mu\text{M}$  of ascorbic acid for 1 month.

by sensing solutions with different dopamine concentrations. As shown in Figure 4c, the DPV peak intensity increases with increasing dopamine concentration. In the range of 0.4–80  $\mu\text{M}$ , the increased peak value  $\Delta I$  showed a linear relationship to dopamine concentration (Figure 4d). The detection limit (DL) could reach  $0.25 \times 10^{-9} \text{ mol L}^{-1}$  ( $DL = 3\delta b/k$ , where  $\delta b$  is the standard deviation of the response and  $k$  is the slope of the calibration curve). The results show that the microtube-based sensor demonstrates higher sensitivity, broad linear detection range (LDR), and low limit of detection compared with those DA sensors reported in previous literature (Table 1). In addition, we also investigated the microtube-based device in sensing ascorbic acid (Figure 5). As schematically shown in Figure 5a, the microtube was coated with Au nanoparticles and further modified with *L*-cysteine (LCY).<sup>40</sup> The peak at  $1594 \text{ cm}^{-1}$  (bending vibration of  $\text{NH}_2$ ) disappears in the corresponding FTIR spectrum of microtube after modification indicates that LCY was successfully assembled

onto the microtube surface (Figure 5b). In addition, as shown in Figure 5c, the DPV peak value increases with the increasing ascorbic acid concentration. In the range of 1–300  $\mu\text{M}$ , the increased peak value ( $\Delta I$ ) also exhibits a linear relationship to ascorbic acid (Figure 5d). To further confirm the advantage of microtubular geometry, current–time ( $i$ – $t$ ) tests of sensor devices made from nanomembranes and microtubes with successive addition of 1 mM DA and 1 mM AA were carried out. As shown in Figure S10, little current response can be observed in the case of flat nanomembranes, revealing their poor electrochemical activity. On the contrary, obvious current steps are observed for microtubes, suggesting the strong sensing activity of microtube-based sensor toward DA and AA oxidation.

To investigate the selectivity of the scroll sensor for dopamine and ascorbic acid determination, the interferences of some potential ions in real samples should be tested. In our work, NaCl, KCl, CaCl<sub>2</sub>, glucose, *o*-phenylenediamine (OPD),

hydroquinone (HQ), and catechol were used as the interferences, and the results are shown in Figure 6a and Figure 6b. One can see that these interferents have no influence (electrical signal change within  $\pm 5\%$ ) on the detection of  $5 \mu\text{M}$  dopamine and  $20 \mu\text{M}$  ascorbic acid in terms of the current response of the interferents when the concentrations of interferents are only 1/10 of the concentration of target molecule. These results further verify the great anti-interference property and stability of the microtube-based sensor. The reproducibility of the sensor was evaluated by sensing  $5 \mu\text{M}$  dopamine by using five sensors prepared by the same approach. The relative standard limits (RSD) were 2.45% (Figure 6c), proving the good reproducibility of the sensor. In addition, the stability of the sensor was also tested. As shown in Figure 6d, the current values of the sensor after 1, 3, 5, 7, 9, and 12 days show slight change (within  $\pm 5\%$ ), indicating the good stability. In order to further investigate the practical application of microtube sensor, 1 mL of human urine (containing DA) or 1 mL of lemon juice (containing AA) is successively added. As shown in Figure S11, both the addition of urine and the addition of lemon juice can lead to significant current response, indicating the applicability of the microtube sensors in detecting target molecules in real samples.

We consider that the outstanding sensing property of our sensor can be attributed to its unique structural properties. First, rolled microstructures have strong confinement to target molecules, which is beneficial to the sensing performance. Second, the rough surface of Janus nanomembrane with exposure of more active sites improves the effect of combination of probe with target molecules,<sup>23</sup> which remarkably enhances the selectivity and sensitivity of sensor. Third, the ultrathin nanomembrane as well as the deposition of Au nanoparticles enhances the ion transfer efficiency, leading to fast response to target molecules.<sup>24</sup>

## CONCLUSION

In this study, oxides Janus nanomembranes and corresponding rolled microtubes have been prepared based on ALD combined with ultrasonication treatment. The free-standing nanomembranes with one-side porosity can be transformed from planar state to microtubular structure in solvent of large polarity with the help of ultrasonication. Functionalized microtubes were developed for applications in electrochemical sensing. Due to their unique geometrical structure, the sensors demonstrate superior selectivity and great sensing property toward DA and AA in terms of low limit of detection and wide linear range. The stability of the sensor was also demonstrated as it remains comparable sensing property after 12 days. The tubular structure, the porous inner surface, and the exposure of active sites are considered to be the main originations of the outstanding performance. The current approach provides an effective way to prepare novel 3D sensing structures and may have great potential in the future.

## EXPERIMENTAL SECTION

**Preparation of Metal Oxide Nanomembranes.** Oxide nanomembranes were prepared by ALD. Here, a sponge skeleton was used as a sacrificial template. The deposition of  $\text{TiO}_2$  nanomembranes on the template was conducted at  $100 \text{ }^\circ\text{C}$  in a homemade reactor. Tetrakis(dimethylamido)titanium (TDMAT) was employed as a Ti source, and water was used as oxygen source. A typical ALD cycle includes TDMAT pulse (60 ms), waiting time (3 s),  $\text{N}_2$  purge (20 s),  $\text{H}_2\text{O}$  pulse (30 ms), waiting time (2 s), and  $\text{N}_2$  purge (20 s).  $\text{N}_2$  gas

served as both the carrier and purge gas.  $\text{TiO}_2$  layer was coated on the surfaces of the template with different cycles. Then, the samples were annealed at  $450 \text{ }^\circ\text{C}$  for 1 h under an  $\text{O}_2$  flow to remove the sponge template, then  $\text{TiO}_2$  spongy structure was formed, and after manual crashing, a large amount of  $\text{TiO}_2$  nanomembranes have been fabricated. In our work, ZnO and  $\text{Al}_2\text{O}_3$  nanomembranes were also obtained by a similar approach, while diethylzinc and trimethylaluminum were employed as Zn and Al sources, respectively.

**Preparation of Metal Oxide Microtubes.** The obtained oxide nanomembranes were put in ethanol for 1 min to elute organic residue, then immersed in water for sonication (2 h, 100 kHz). The microtubes were then obtained.

**Fabrication of Sensing Microtubes.** The prepared ethanol solution of microtubes ( $0.2 \text{ mg L}^{-1}$ ) was dispersed in Nafion (0.03%), and then  $4.0 \mu\text{L}$  of dispersion was dropped on the surface of a glassy carbon (GC) electrode. The GC was dried at room temperature for 4 h. Next, functional layers were deposited on the surface of microtubes. For example, the dopamine sensing microtubes were constructed by electrodepositing CBK as a mediator to provide better sensitivity. The ascorbic acid sensing microtubes were obtained with gold nanoparticles as accelerated chemical reactor. The device was further modified with LCY.

**Electrochemical Sensor Fabrication.** Working electrodes were prepared by modified glassy carbon electrodes with the microtubes binding LCY or CBK (Figure S12a). An Ag/AgCl (in saturated KCl solution) was used as the reference electrode, and a graphite rod was used as the counter electrode (see the photograph in Figure S12). The devices were placed at room temperature for the subsequent tests.

**Structural Characterizations.** The surface morphologies of nanomembranes and microtubes were inspected by SEM (JEOL JSM-6701F). The elemental composition and characteristic functional groups of the scrolls were analyzed by FTIR spectrometer (Nicolet 6700, ThermoFisher). The EIS characterizations were carried out in  $0.05 \text{ mol L}^{-1} \text{ K}_3[\text{Fe}(\text{CN})_6]/\text{K}_4[\text{Fe}(\text{CN})_6]$  containing  $0.5 \text{ mol L}^{-1}$  KCl and with the alternating voltage of 5 mV in the frequency range of 0.1–100 000 Hz.

**Electrochemical Characterizations.** All the biosensing tests were carried out on an electrochemical workstation (PGSTAT128N Autolab). The detection procedure was performed by a DPV method in the potential range of 0–0.8 V and with the scanning rate of  $0.1 \text{ V s}^{-1}$  in a Tris-HCl solution (pH = 7.0) containing targets of various concentrations. The sensor was then successively aged until 1 month. When not in use, the sensor was stored in a refrigerator at  $6 \text{ }^\circ\text{C}$ .

## ASSOCIATED CONTENT

### Supporting Information

The Supporting Information is available free of charge at <https://pubs.acs.org/doi/10.1021/acsnm.0c02019>.

Additional microscopy images, statistics of microtube formation, XRD pattern, XPS results, particle size distribution,  $i-t$  curves, and fitting parameters of EIS (PDF)

## AUTHOR INFORMATION

### Corresponding Authors

Gaoshan Huang – Department of Materials Science, Fudan University, Shanghai 200433, People's Republic of China; [orcid.org/0000-0002-0525-7177](https://orcid.org/0000-0002-0525-7177); Email: [gshuang@fudan.edu.cn](mailto:gshuang@fudan.edu.cn)

Yongfeng Mei – Department of Materials Science, Fudan University, Shanghai 200433, People's Republic of China; [orcid.org/0000-0002-3314-6108](https://orcid.org/0000-0002-3314-6108); Email: [yfm@fudan.edu.cn](mailto:yfm@fudan.edu.cn)

## Authors

- Fei Ma** – Department of Materials Science, Fudan University, Shanghai 200433, People's Republic of China
- Bin Yang** – Department of Chemistry, Fudan University, Shanghai 200433, People's Republic of China
- Zhe Zhao** – Department of Materials Science, Fudan University, Shanghai 200433, People's Republic of China
- Yuting Zhao** – Department of Materials Science, Fudan University, Shanghai 200433, People's Republic of China
- Ruobing Pan** – Department of Materials Science, Fudan University, Shanghai 200433, People's Republic of China
- Dingrun Wang** – Department of Materials Science, Fudan University, Shanghai 200433, People's Republic of China
- Ye Kong** – Department of Materials Science, Fudan University, Shanghai 200433, People's Republic of China
- Yimeng Chen** – Department of Materials Science, Fudan University, Shanghai 200433, People's Republic of China
- Jilie Kong** – Department of Chemistry, Fudan University, Shanghai 200433, People's Republic of China

Complete contact information is available at:  
<https://pubs.acs.org/10.1021/acsnm.0c02019>

## Notes

The authors declare no competing financial interest.

## ACKNOWLEDGMENTS

This work is supported by Natural Science Foundation of China (Grants 51961145108 and 61975035), Science and Technology Commission of Shanghai Municipality (Grants 19XD1400600 and 17JC1401700), and China National Postdoctoral Program for Innovative Talents (Grant BX2020090).

## REFERENCES

- (1) Liu, Y.; Shaw, B.; Dickey, M. D.; Genzer, J. Sequential Self-folding of Polymer Sheets. *Sci. Adv.* **2017**, *3*, e1602417.
- (2) Zhao, Z.; Liu, S. L.; Zhu, J. X.; Xu, J. S.; Li, L.; Huang, Z. Q.; Zhang, C.; Liu, T. X. Hierarchical Nanostructures of Nitrogen-Doped Porous Carbon Polyhedrons Confined in Carbon Nanosheets for High-Performance Supercapacitors. *ACS Appl. Mater. Interfaces* **2018**, *10*, 19871–19880.
- (3) Zhang, Z. W.; Deng, L. J.; Zhao, Z.; Zhao, Y. T.; Yang, J. Y.; Jiang, J.; Huang, G. S.; Mei, Y. F. Nickel Nanograins Anchored On a Carbon Framework For an Efficient Hydrogen Evolution Electrocatalyst and a Flexible Electrode. *J. Mater. Chem. A* **2020**, *8*, 3499–3508.
- (4) Ansari, N.; Payami, Z. Synthesis of Magnetic Graphene-Fe<sub>3</sub>O<sub>4</sub> Nanocomposite by Electrochemical Exfoliation Method. *J. Nanostruct.* **2020**, *10*, 39–43.
- (5) Yan, Z.; Wang, W.; Du, L.; Zhu, J.; Phillips, D. L.; Xu, J. Interpreting the Enhanced Photoactivities of 0D/1D Heterojunctions of CdS Quantum Dots /TiO<sub>2</sub> Nanotube Arrays Using Femtosecond Transient Absorption Spectroscopy. *Appl. Catal., B* **2020**, *275*, 119151.
- (6) Georgakilas, V.; Perman, J. A.; Tucek, J.; Zboril, R. Broad Family of Carbon Nanoallotropes: Classification, Chemistry, and Applications of Fullerenes, Carbon Dots, Nanotubes, Graphene, Nanodiamonds, and Combined Superstructures. *Chem. Rev.* **2015**, *115*, 4744–4822.
- (7) Li, F.; Song, Q.; Zhang, X. Two-Dimensional Folded Nanosheets Lead to an Unusual Circular Dichroism Effect in Aqueous Solution. *Langmuir* **2014**, *30*, 6064–6070.
- (8) Wang, L.; Tian, Z.; Zhang, B.; Xu, B.; Wang, T.; Wang, Y.; Li, S.; Di, Z.; Mei, Y. On-Chip Rolling Design for Controllable Strain Engineering and Enhanced Photon-Phonon Interaction in Graphene. *Small* **2019**, *15*, 1805477.
- (9) Berman, D.; Deshmukh, S. A.; Sankaranarayanan, S. K. R. S.; Erdemir, A.; Sumant, A. V. Macroscale Superlubricity Enabled by Graphene Nanoscroll Formation. *Science* **2015**, *348*, 1118–1122.
- (10) Wu, B.; Zhang, G.; Yan, M.; Xiong, T.; He, P.; He, L.; Xu, X.; Mai, L. Graphene Scroll-Coated alpha-MnO<sub>2</sub> Nanowires as High-Performance Cathode Materials for Aqueous Zn-Ion Battery. *Small* **2018**, *14*, 1703850.
- (11) Yan, M.; Wang, F.; Han, C.; Ma, X.; Xu, X.; An, Q.; Xu, L.; Niu, C.; Zhao, Y.; Tian, X.; Hu, P.; Wu, H.; Mai, L. Nanowire Templated Semihollow Bicontinuous Graphene Scrolls: Designed Construction, Mechanism, and Enhanced Energy Storage Performance. *J. Am. Chem. Soc.* **2013**, *135*, 18176–18182.
- (12) Zeng, F.; Kuang, Y.; Wang, Y.; Huang, Z.; Fu, C.; Zhou, H. Facile Preparation of High-Quality Graphene Scrolls from Graphite Oxide by a Microexplosion Method. *Adv. Mater.* **2011**, *23*, 4929–4932.
- (13) Naeem, F.; Naeem, S.; Zhao, Z.; Shu, G.; Zhang, J.; Mei, Y. F.; Huang, G. S. Atomic Layer Deposition Synthesized ZnO Nanomembranes: A Facile Route Towards Stable Supercapacitor Electrode for High Capacitance. *J. Power Sources* **2020**, *451*, 227740.
- (14) Wu, X.; Xiong, S.; Liu, Z.; Chen, J.; Shen, J.; Li, T.; Wu, P.; Chu, P. Green Light Stimulates Terahertz Emission From Mesocrystal Microspheres. *Nat. Nanotechnol.* **2011**, *6*, 103–106.
- (15) Bai, J.; Zhou, B. Titanium Dioxide Nanomaterials for Sensor Applications. *Chem. Rev.* **2014**, *114*, 10131–10176.
- (16) Xu, C.; Shin, P. H.; Cao, L.; Wu, J.; Gao, D. Ordered TiO<sub>2</sub> Nanotube Arrays on Transparent Conductive Oxide for Dye-Sensitized Solar Cells. *Chem. Mater.* **2010**, *22*, 143–148.
- (17) Yun, J.; Mozer, A. J.; Wagner, P.; Offier, D. L.; Amal, R.; Ng, Y. H. Light Soaking Effect Driven in Porphyrin Dye-Sensitized Solar Cells Using 1D TiO<sub>2</sub> Nanotube Photoanodes. *Sustainable Mater. Technol.* **2020**, *24*, e00165.
- (18) Liu, W.; Zhang, L.; Cao, L.-X.; Su, G.; Wang, Y.-G. Glass Fibers Templated Preparation of TiO<sub>2</sub> Microtubes Assembled From Nano/micro Hierarchical TiO<sub>2</sub> Crystals. *J. Alloys Compd.* **2011**, *509*, 3419–3424.
- (19) Zhao, Z.; Kong, Y.; Zhang, Z. W.; Huang, G. S.; Mei, Y. F. Atomic Layer-Deposited Nanostructures and Their Applications in Energy Storage and Sensing. *J. Mater. Res.* **2020**, *35*, 701–719.
- (20) Liu, B.; Wang, X.; Liu, H.; Zhai, Y.; Li, L.; Wen, H. 2D MOF with Electrochemical Exfoliated Graphene for Nonenzymatic Glucose Sensing: Central Metal Sites and Oxidation Potentials. *Anal. Chim. Acta* **2020**, *1122*, 9–19.
- (21) Karimi-Maleh, H.; Cellat, K.; Arkan, K.; Savk, A.; Karimi, F.; Sen, F. Palladium-Nickel Nanoparticles Decorated on Functionalized-MWCNT for High Precision Non-enzymatic Glucose Sensing. *Mater. Chem. Phys.* **2020**, *250*, 123042.
- (22) Di, X.; Pan, Y.; Dai, W.; Zhu, Y.-a.; Lu, T. In -situ Electrochemical Oxidation of Amorphous Nanoporous NiZrO for Enhanced Non-enzymatic Glucose Sensing. *Mater. Lett.* **2020**, *271*, 127694.
- (23) Li, Y.; Xie, G.; Qiu, J.; Zhou, D.; Gou, D.; Tao, Y.; Li, Y.; Chen, H. A new biosensor based on the recognition of phages and the signal amplification of organic-inorganic hybrid nanoflowers for discriminating and quantitating live pathogenic bacteria in urine. *Sens. Actuators, B* **2018**, *258*, 803–812.
- (24) Qing, X.; Wang, Y.; Zhang, Y.; Ding, X.; Zhong, W.; Wang, D.; Wang, W.; Liu, Q.; Liu, K.; Li, M.; Lu, Z. Wearable Fiber-Based Organic Electrochemical Transistors as a Platform for Highly Sensitive Dopamine Monitoring. *ACS Appl. Mater. Interfaces* **2019**, *11*, 13105–13113.
- (25) Reddy, S.; Xiao, Q.; Liu, H.; Li, C.; Chen, S.; Wang, C.; Chiu, K.; Chen, N.; Tu, Y.; Ramakrishna, S.; He, L. Bionanotube/Poly(3,4-ethylenedioxythiophene) Nanohybrid as an Electrode for the Neural Interface and Dopamine Sensor. *ACS Appl. Mater. Interfaces* **2019**, *11*, 18254–18267.

- (26) Li, G.; Liang, H.; Xu, G.; Li, C.; Bai, J. Controllable Synthesized Heterojunction Hollow Nanotube of g-C<sub>3</sub>N<sub>4</sub>/CdS: Enhance Visible Light Catalytic Performance for Hydrogen Production. *J. Phys. Chem. Solids* **2020**, *145*, 109549.
- (27) Kong, X.; Li, J.; Yang, C.; Tang, Q.; Wang, D. Fabrication of Fe<sub>2</sub>O<sub>3</sub>/g-C<sub>3</sub>N<sub>4</sub>@N-TiO<sub>2</sub> Photocatalyst Nanotube Arrays that Promote Bisphenol A Photodegradation Under Simulated Sunlight Irradiation. *Sep. Purif. Technol.* **2020**, *248*, 116924.
- (28) Hiltunen, A.; Lahtonen, K.; Saari, J.; Ojanpera, A.; Sarlin, E.; Wondraczek, H.; Efimov, A.; Kaunisto, K.; Vivo, P.; Maccato, C.; Barreca, D.; Fardim, P.; Tkachenko, N.; Valden, M.; Lemmetyinen, H. Tailored Fabrication of Transferable and Hollow Weblike Titanium Dioxide Structures. *ChemPhysChem* **2017**, *18*, 64–71.
- (29) Lepcha, A.; Maccato, C.; Mettenboerger, A.; Andreu, T.; Mayrhofer, L.; Walter, M.; Olthof, S.; Ruoko, T. P.; Klein, A.; Moseler, M.; Meerholz, K.; Morante, J. R.; Barreca, D.; Mathur, S. Electrospun Black Titania Nanofibers: Influence of Hydrogen Plasma-Induced Disorder on the Electronic Structure and Photoelectrochemical Performance. *J. Phys. Chem. C* **2015**, *119*, 18835–18842.
- (30) Xu, J.; Dai, W.-L.; Li, J.; Cao, Y.; Li, H.; He, H.; Fan, K. Simple Fabrication of Thermally Stable Apertured N-doped TiO<sub>2</sub> Microtubes as a Highly Efficient Photocatalyst Under Visible Light Irradiation. *Catal. Commun.* **2008**, *9*, 146–152.
- (31) Viculis, L. M.; Mack, J. J.; Kaner, R. B. A Chemical Route to Carbon Nanoscrolls. *Science* **2003**, *299*, 1361–1361.
- (32) Mei, Y. F.; Huang, G. S.; Solovev, A. A.; Urena, E. B.; Moench, I.; Ding, F.; Reindl, T.; Fu, R. K. Y.; Chu, P. K.; Schmidt, O. G. Versatile Approach for Integrative and Functionalized Tubes by Strain Engineering of Nanomembranes on Polymers. *Adv. Mater.* **2008**, *20*, 4085–4090.
- (33) Ma, F.; Xu, B. R.; Wu, S.; Wang, L.; Zhang, B. R.; Huang, G. S.; Du, A.; Zhou, B.; Mei, Y. F. Thermal-Controlled Releasing and Assembling of Functional Nanomembranes Through Polymer Pyrolysis. *Nanotechnology* **2019**, *30*, 354001.
- (34) Hu, C.; Zhao, Y.; Cheng, H.; Wang, Y.; Dong, Z.; Jiang, C.; Zhai, X.; Jiang, L.; Qu, L. Graphene Microtubings: Controlled Fabrication and Site-Specific Functionalization. *Nano Lett.* **2012**, *12*, 5879–5884.
- (35) Pan, S.; Zhao, Y.; Huang, G.; Wang, J.; Baunack, S.; Gemming, T.; Li, M.; Zheng, L.; Schmidt, O. G.; Mei, Y. Highly Photocatalytic TiO<sub>2</sub> Interconnected Porous Powder Fabricated by Sponge-Templated Atomic Layer Deposition. *Nanotechnology* **2015**, *26*, 364001–364001.
- (36) Zhao, Z.; Zhang, Z. W.; Zhao, Y. T.; Liu, J. R.; Liu, C.; Wang, Z. J.; Zheng, G. F.; Huang, G. S.; Mei, Y. F. Atomic Layer Deposition Inducing Integration of Co, N Codoped Carbon Sphere on 3D Foam with Hierarchically Porous Structures for Flexible Hydrogen Producing Device. *Adv. Funct. Mater.* **2019**, *29*, 1906365.
- (37) Zhao, Z.; Kong, Y.; Liu, C.; Liu, J. R.; Wang, Z. J.; Zheng, G. F.; Huang, G. S.; Mei, Y. F. Atomic Layer Deposition-Induced Integration of N-doped Carbon Particles on Carbon Foam for Flexible Supercapacitor. *J. Mater. Chem.* **2020**, *6*, 209–215.
- (38) Li, X.; Luo, D.; Zhang, X.; Zhang, Z. Enhancement of Electrochemical Performances for LiFePO<sub>4</sub>/C with 3D-grape-bunch Structure and Selection of Suitable Equivalent Circuit for Fitting EIS Results. *J. Power Sources* **2015**, *291*, 75–84.
- (39) Arroquia, A.; Acosta, I.; Garcia Armada, M. P. Self-assembled Gold Decorated Polydopamine Nanospheres as Electrochemical Sensor for Simultaneous Determination of Ascorbic Acid, Dopamine, Uric Acid and Tryptophan. *Mater. Sci. Eng., C* **2020**, *109*, 110602.
- (40) Jothi, L.; Neogi, S.; Jaganathan, S. K.; Nageswaran, G. Simultaneous Determination of Ascorbic Acid, Dopamine and Uric Acid by A Novel Electrochemical Sensor Based on N-2/Ar RF Plasma Assisted Graphene Nanosheets/Graphene Nanoribbons. *Biosens. Bioelectron.* **2019**, *129*, 298–298.
- (41) How, G.; Pandikumar, A.; Ming, H. N.; Ngee, L. H. Highly Exposed {001} Facets of Titanium Dioxide Modified with Reduced Graphene Oxide for Dopamine Sensing. *Sci. Rep.* **2014**, *4*, 5044.
- (42) Reddy, S.; Swamy, B. E. K.; Jayadevappa, H. CuO Nanoparticle Sensor for The Electrochemical Determination of Dopamine. *Electrochim. Acta* **2012**, *61*, 78–86.
- (43) Zhang, S.; Fu, Y.; Sheng, Q.; Zheng, J. Nickel-Cobalt Double Hydroxide Nanosheets Wrapped Amorphous Ni(OH)<sub>2</sub> Nanoboxes: Development of Dopamine Sensor with Enhanced Electrochemical Properties. *New J. Chem.* **2017**, *41*, 13076–13084.
- (44) Lin, X.; Zhuang, Q.; Chen, J.; Zhang, S.; Zheng, Y. Electrochemical Property of Poly-chromotrope 2B Modified Glassy Carbon Electrode on Dopamine and its Application. *Sens. Actuators, B* **2007**, *125*, 240–245.
- (45) Alarcon-Angeles, G.; Perez-Lopez, B.; Palomar-Pardave, M.; Ramirez-Silva, M.T.; Alegret, S.; Merkoci, A. Enhanced Host-Guest Electrochemical Recognition of Dopamine Using Cyclodextrin in the Presence of Carbon Nanotubes. *Carbon* **2008**, *46*, 898–906.
- (46) Zheng, G.; Chen, M.; Liu, X.; Zhou, J.; Xie, J.; Diao, G. Self-assembled Thiolated Calix n arene (n = 4, 6, 8) Films on Gold Electrodes and Application for Electrochemical Determination Dopamine. *Electrochim. Acta* **2014**, *136*, 301–309.
- (47) Baruah, U.; Gogoi, N.; Konwar, A.; Jyoti Deka, M.; Chowdhury, D.; Majumdar, G. Carbon Dot Based Sensing of Dopamine and Ascorbic Acid. *J. Nanopart.* **2014**, 178518.
- (48) Gao, W.; Ye, S.; Shao, M. Solution-Combusting Preparation of Mono-Dispersed Mn<sub>3</sub>O<sub>4</sub> Nanoparticles for Electrochemical Applications. *J. Phys. Chem. Solids* **2011**, *72*, 1027–1031.
- (49) Cui, L.; Zou, Y.; Lin, N.; Zhu, Z.; Jenkins, G.; Yang, C. J. Mass Amplifying Probe for Sensitive Fluorescence Anisotropy Detection of Small Molecules in Complex Biological Samples. *Anal. Chem.* **2012**, *84*, 5535–5541.
- (50) Yu, D.; Zeng, Y.; Qi, Y.; Zhou, T.; Shi, G. A Novel Electrochemical Sensor for Determination of Dopamine Based on AuNPs@SiO<sub>2</sub> Core-shell Imprinted Composite. *Biosens. Bioelectron.* **2012**, *38*, 270–277.